

# Iterative Exponential Growth of Oxygen-linked Aromatic Polymers Driven by Nucleophilic Aromatic Substitution Reactions

- 3 Tyler J. Jaynes<sup>#1</sup>, Mona Sharafi<sup>#1</sup>, Joseph P. Campbell<sup>#1</sup>, Jessica Bocanegra<sup>1</sup>, Kyle T. McKay<sup>1</sup>,
- 4 Kassondra Little<sup>1</sup>, Reilly Osadchey Brown<sup>1</sup>, Danielle L. Gray<sup>2</sup>, Toby J. Woods<sup>2</sup>, Jianing Li<sup>1</sup>,
- 5 and Severin T. Schneebeli\*1
- 6 Department of Chemistry, University of Vermont, Burlington, VT 05405, USA
- <sup>2</sup>George L. Clark X-Ray Facility & 3M Materials Laboratory, University of Illinois at Urbana-
- 8 Champaign, Urbana, IL 61801, USA
- 9 # Equal Authorship Contribution
- 10 \* Correspondence:
- 11 Severin T. Schneebeli
- 12 severin.schneebeli@uvm.edu
- 13 **Keywords:** Iterative convergent/divergent polymer synthesis, S<sub>N</sub>Ar reactions, non-classical hydrogen
- bonding, nuclear magnetic resonance spectroscopy, polymer folding, iterative exponential polymer
- 15 growth, transition metal-free coupling

#### 16 Abstract

17

18

19

20

21

22

23

24

25

26

27

28

macromolecules.

1

2

This work presents the first transition metal-free synthesis of oxygen-linked aromatic polymers by integrating iterative exponential polymer growth (IEG) with nucleophilic aromatic substitution (S<sub>N</sub>Ar) reactions. Our approach applies methyl sulfones as the leaving groups, which eliminates the need for a transition-metal catalyst, while also providing flexibility in functionality and configuration of the building blocks used. As indicated by (i) <sup>1</sup>H-<sup>1</sup>H NOESY NMR spectroscopy, (ii) single crystal X-ray crystallography, and (iii) density functional theory (DFT) calculations, the unimolecular polymers obtained are folded by non-classical hydrogen bonds formed between the oxygens of the electron rich aromatic rings and the positively-polarized C–H bonds of the electron poor pyrimidine functions. Our results not only introduce a transition metal-free synthetic methodology to access precision polymers, but also demonstrate how interactions between relatively small, neutral aromatic units in the polymers can be utilized as a new supramolecular interaction pairs to control the folding of precision

### 1 Introduction

The backbones of conjugated and heteroatom-linked aromatic polymers tend to possess fewer conformational degrees of freedom than polymers with more flexible aliphatic or partially-aliphatic backbones. This reduced amount of conformational freedom can help enhance the folding of aromatic polymers, to advance a variety of useful properties such as selective supramolecular recognition (Goodman et al., 2007; Liu et al., 2015; Otte, 2016; Schneebeli et al., 2016; Adhikari et al., 2017; Xie et al., 2020), selective catalysis (Rajappan et al., 2020; Sharafi et al., 2020) and self-assembly (Cole et al., 2017; Greene et al., 2017; Bonduelle, 2018; Ong and Swager, 2018; Delawder et al., 2019; Zhao et al., 2019). However, while the precise chemical structures, lengths, and sequences of such macromolecules (Dobscha et al., 2019; Gerthoffer et al., 2020; Zhao et al., 2020) dictates their folding, and with it their functionalities and physical properties (Chen et al., 2015; Hanlon et al., 2017) it remains challenging to synthesize polyaromatic structures with precise lengths and/or sequences as unimolecular entities. One of the most efficient ways to precisely control the length and sequence of synthetic polymers is by iteratively coupling (Jones et al., 1997) polymer strands together in a convergent/divergent fashion (Hawker et al., 1997; Read et al., 2000; Grayson and Frechet, 2001; Li et al., 2005; Liess et al., 2006; Binauld et al., 2011). This methodology (Figure 1) is generally referred to as iterative exponential growth (Barnes et al., 2015; Leibfarth et al., 2015).

IEG requires a dormant monomer that includes two distinct functionalities, which are orthogonally deprotected/activated for coupling, to afford two reactive species that can be coupled to together selectively. These two reactive species are then combined in a chemo-selective manner, resulting in a dormant dimer, which contains, again, protected/masked functionalities identical to the original dormant monomer (Figure 1). Repeating this simple protocol results in the creation of architecturally defined structures with an exponential gain in polymer length. The IEG method has been applied extensively to synthesize flexible linear polymers (Barnes et al., 2015; Huang et al., 2017)— e.g. via copper-catalyzed azide-alkyne click (CuAAC) reactions. However, it still remains a challenge to efficiently utilize arylation chemistry with an IEG-reaction framework, as is required in order to access conjugated or heteroatom-linked polyaromatic polymers with IEG methodology. In particular, while transition metal-catalyzed arylation reactions have been utilized previously to synthesize conjugated and/or heteroatom-linked polyaromatic macromolecules (Figure 1), (Zhang et al., 1992; Louie and Hartwig, 1998; Sadighi et al., 1998; Liess et al., 2006) there are (to the best of our knowledge) currently no transition metal-free reactions available to achieve exponential polymer growth for conjugated or heteroatom-linked polyaromatic structures. We were now able to meet this synthetic challenge by

marrying iterative exponential polymer growth with nucleophilic aromatic substitution ( $S_NAr$ ) reactions (Beugelmans et al., 1994; Blaziak et al., 2016; Landovsky et al., 2019) with a unique masking/unmasking technique. Unmasking was achieved by simply oxidizing aromatic sulfides to sulfones — a mild, simple, and scalable reaction well-suited for IEG applications. At the same time, the IEG coupling reactions also proceeded under mild conditions (mild heating to  $\sim 50$  °C), which represents an advantage over transition metal-catalyzed alternatives (which tend to require stronger heating (Sadighi et al., 1998).

Our new synthetic technology for precision polymer growth helps resolve a number of concerns, which exist with traditional, transition metal-catalyzed cross-coupling methodology (Sun et al., 2014; Li et al., 2020). These issues include, but are not limited to: (i) The inherent toxicity of many transition metal catalysts, which goes hand in hand with the need to accomplish/demonstrate complete removal of any residual transition metal, especially for healthcare-related applications (which can be difficult to achieve with polymers containing many Lewis basic groups like the ones presented in this paper), (ii) the relatively high cost of the required transition-metal catalysts and complex ligands, which are often needed for high-yielding cross-coupling reactions suitable for polymer growth. Transition metal-free cross-coupling protocols like the one presented in this paper have the potential to overcome these fundamental challenges associated with transition metal-catalyzed polymer growth.

### 2 Results and Discussion

To implement our new sulfide oxidation-driven IEG coupling strategy, we first tested a variety of sulfone leaving groups for their ability to couple with phenolate anions in our IEG scheme (for related work, see: Guan et al., 2015). We discovered that simple methyl sulfones (Figure 1) are best suited for this purpose as with sulfone substituents larger than methyl (e.g. phenyl), we tended to get lower IEG coupling yields. For our synthetic scheme, we decided to protect the phenols with methyl groups (which can readily be removed in high yield with BBr<sub>3</sub>). However, it is very likely that instead of just methyl groups, alternative phenol protection groups (e.g. benzyl) can also be also be utilized in the future to further enhance the functional-group tolerance of our IEG coupling scheme. To start our IEG couplings, we first condensed 3-methoxyphenol with 4-chloro-6-(methylthio)pyrimidine in quantitative yield under standard S<sub>N</sub>Ar conditions with K<sub>2</sub>CO<sub>3</sub> as the base (Van Rossom et al., 2012). The resulting dimeric product 4-(3-methoxyphenoxy)-6-(methylthio)pyrimidine (3) was then split in half for the next IEG deprotection/activation/coupling cycle. The first aliquot was subjected to BBr<sub>3</sub> for methoxyl deprotection, while the second aliquot was activated via oxidization to the methyl sulfone

92

93 IEG coupling, again in the presence of K<sub>2</sub>CO<sub>3</sub> as the base. Ultimately, by iteratively implementing 94 (Scheme 1) our new, transition-metal free IEG methodology, we were able to access macromolecules 95 with up to 16 perfectly alternating AB units — where A and B represent resorcinol and pyrimidine 96 rings — for the first time in a fully unimolecular fashion. 97 We hypothesized that the electron-deficient pyrimidine units in our unimolecular oligomers might be 98 able to promote folding (Scheme 1, inset) via hydrogen-bonding of and/or  $\pi$ -stacking with the electron 99 rich resorcinol units. To investigate this hypothesis, we grew single-crystals suitable for single crystal 100 X-ray diffraction analysis of compound 3 by slow vapor diffusion of hexanes into ethyl 101 acetate solutions of 3. The packing observed (Figure 2A–B) upon analysis of the diffraction pattern of 102 a single crystal of compound 3 clearly demonstrates the ability of the positively-polarized -N=CH-N= 103 hydrogens in the pyridimidine rings to form intermolecular hydrogen bonds with the methoxyl group 104 of another molecule of 3 in the solid state. There are other hydrogen-bonding interactions that are less 105 strong, but still significant, that also contribute (see supplementary Table S1) to the supramolecular 106 packing of this structure. To estimate the strength of the [pyrimidine-CH···OCH<sub>3</sub>] hydrogen bonds 107 observed in the crystal structure of 3, we optimized a model dimer — 1,3-dimethoxyphenol in complex 108 with 4-methoxy-6-(methylthio)pyrimidine — with density functional theory at the B3LYP(Lee et al., 109 1988; Becke, 1993)/6-31G\*\* level of theory. Next we used the noncovalent interactions (NCI) code 110 (Johnson et al., 2010) implemented in the Jaguar (Bochevarov et al., 2013) software package to find 111 all major attractive supramolecular interactions present in our model dimer, characterized as critical 112 points of the electron density. The NCI critical points of the DFT-optimized structure of the model 113 dimer (Figure 2C) clearly show the presence of a [pyrimidine-CH···OCH<sub>3</sub>], with a strength of ~5.8 114 kcal/mol. 115 Having established that the pyridimide rings are attracted to the resorcinol units in the solid state via 116 [CH···O] hydrogen bonding, we next embarked on investigating the ability of the polymer 6 — the 117 longest unimolecular, alternating pyrimidine/resorcinol polymer synthesized to date — to fold, driven 118 by [CH···O] hydrogen bonding interactions. To demonstrate folding, we recorded a <sup>1</sup>H-<sup>1</sup>H NOESY 119 NMR spectrum of the hexadecamer 6 in CDCl<sub>3</sub> at 298 K. The <sup>1</sup>H-<sup>1</sup>H NOESY NMR spectrum displays 120 (Figure 3A) a NOE cross peak between the proton resonance x of the terminal methoxyl group and the 121 -NCHN- proton resonances ( $b^1$ - $b^7$ , which all overlap at the same resonance frequency at 8.48 ppm). 122 Notably, this NOE cross peak is absent in the <sup>1</sup>H-<sup>1</sup>H NOESY NMR spectrum of the dimer 3

with mCPBA. Following these deprotection/activation steps, we were able to perform an S<sub>N</sub>Ar-based

123 (Figure S1), which demonstrates that folding and/or supramolecular aggregation (and not just simply 124 the fact that the proton corresponding to resonance  $b^7$  is present in a pyrimidine ring next to the terminal 125 methoxyl group) is responsible for the observed NOE cross peak. Furthermore, a <sup>1</sup>H DOSY NMR 126 spectrum of 6 (Figure S10) confirmed that the compound does not aggregate significantly in solution, 127 and thus the NOE cross peak observed must be stemming from intramolecular folding of the polymer 128 chains. A folded model of the hexadecamer 6 (optimized with DFT at the B3LYP-D3/6-31G\*\* level) 129 is shown in Figure 3B. The structure shown represents the lowest energy conformation obtained from 130 a MacroModel conformational search (carried out without constraints and the state of the art OPLS3e 131 force field (Harder et al., 2016) of the hexadecamer 6. While other potential, folded structures exist, 132 the observed NOE cross peak is consistent with the DFT optimized structure shown in Figure 2B, 133 which shows a [CH...O] hydrogen bonding contact between a pyrimidine CH functionality, and the 134 terminal methoxyl group in 6. For property characterization, we also performed differential scanning 135 calorimetry (DSC) of 6 (see Figure S11 for the DSC thermogram). As 6 is still a relatively low 136 molecular weight compound and fully unimolecular, we did not observe any phase transitions in the 137 temperature range investigated (30–335 °C).

Overall, our results demonstrate that methyl sulfones can be effective leaving groups for transition metal free, iterative exponential growth processes. Furthermore, the electrophilic pyrimidine cores present in our polymers not only help further enhance the yields for the S<sub>N</sub>Ar-based IEG coupling reactions, but also provide strongly polarized C-H bonds, capable of directing the folding of the unimolecular alternating pyrimidine-resorcinol polymers presented in this work.

#### 3 Materials and Methods

143

144

# 3.1 General Methods and Materials of Synthesis

145 All commercially available starting materials were purchased from Sigma Aldrich, Fisher Scientific, 146 or Oakwood Chemical. Unless notes otherwise, all reagents were used as received without further 147 purification. When needed dichloromethane (CH<sub>2</sub>Cl<sub>2</sub>) and dimethylformamide (DMF) were dried 148 using a Glass Contour solvent purification system by SG Water USA, LLC. Removal of solvents was 149 accomplished on a Büchi R-210 rotary evaporator and further concentration was attained under a Fisher 150 Scientific Maxima C-Plus vacuum line. Column chromatography was performed manually with Sorbent grade 60 silica with a mesh size between 230–400 using a forced flow of indicated solvents, 151 or automatically with a *Teledyne* CombiFlash® Rf+ chromatography system. 152

153 All <sup>1</sup>H NMR spectra and <sup>13</sup>C (<sup>1</sup>H) NMR spectra were recorded on a Bruker ARX 500 (125 MHz) 154 spectrometer and all <sup>1</sup>H-<sup>1</sup>H NOESY NMR were recorded at 298 K on a Varian Unity Inova 500 155 (500 MHz) spectrometer. Samples for NMR spectroscopy were dissolved in CDCl<sub>3</sub> and the spectra were referenced to the residual solvent peak (CDCl<sub>3</sub>: 7.26 ppm for <sup>1</sup>H and 77.16 ppm for 156 <sup>13</sup>C (<sup>1</sup>H) NMR; or to tetramethylsilane (TMS, 0.00 ppm for <sup>1</sup>H and <sup>13</sup>C (<sup>1</sup>H) NMR) as the internal 157 158 standard. Chemical shift values were recorded in parts per million (ppm). Data are reported as follows: 159 chemical shift, multiplicity (s = singlet, d = doublet, t = triplet, q = quartet, m = multiplet, dd = doublet 160 of doublets), coupling constants (Hz), and number of protons. <sup>1</sup>H-<sup>1</sup>H NOESY NMR spectra were 161 acquired with a NOE mixing time of 600 ms. The datasets were processed with MestReNova v10.0.2-162 15465 using Bernstein Polynomial Fits (with a Polynomial order of 3) for baseline corrections. The 163 <sup>1</sup>H DOSY NMR spectra were acquired on a Varian Unity Inova 500 (500 MHz) spectrometer, equipped 164 with a HCN probe with Z-axis gradients, and a Highland Technologies L700 gradient amplifier. The 165 standard DOSY Varian pulse program 'Dbppste' was used, with a stimulated echo sequence and 166 bipolar gradient pulse pairs. All experiments were acquired at 25 °C and DOSY spectra were 167 processed/analyzed using Agilent's VnmrJ (version 4.2) software, employing the discrete approach for 168 the inverse Laplace transform in the diffusion dimension. High resolution mass spectra were obtained 169 on a Waters XEVO G2-XS QTof in positive ESI mode. Differential Scanning Calorimetry (DSC) was 170 performed on a PerkinElmer Pyris 1 differential scanning calorimeter on aluminum plates.

# 3.2 General Synthetic Procedure for the IEG Deprotection/Activation and Coupling Steps

Methoxyl Deprotection: For deprotection of the terminal methoxyl groups, dormant oligomers 3, 4, and 5 (0.224 mmol) were dissolved in anhydrous CH<sub>2</sub>Cl<sub>2</sub> (4 mL) under an atmosphere of dry nitrogen. The reaction mixtures were then cooled to −78 °C and a 1.0 M solution of BBr<sub>3</sub> in CH<sub>2</sub>Cl<sub>2</sub> (0.896 mmol of BBr<sub>3</sub>) was added dropwise via syringe into the stirring solution. Next, the reaction mixtures were allowed to warm to room temperature over the course of ~1 hr, stirred at room temperature for an additional 12 hrs, cooled to 0 °C, and finally quenched by adding MeOH (1 mL) and ice chips until fuming ceased. The mixtures were then added to a separatory funnel and the organic layers were removed. The aqueous layers were extracted with CH<sub>2</sub>Cl<sub>2</sub> (3 x 5 mL) and the combined organic layers were dried over anhydrous Na<sub>2</sub>SO<sub>4</sub>, filtered, and concentrated under reduced pressure to afford the deprotected phenols in 88−98% yield (see also Scheme 1). The free phenols were carried forward for the IEG coupling steps without further purification.

171

172

173

174

175

176

177

178

179

180

181

182

183 Activation of the Electrophilic Coupling Sites via Sulfide Oxidation: Dormant oligomers 3, 4, and 184 5 (0.23 mmol) were dissolved in anhydrous EtOAc (4 mL) and a solution of 70% meta-185 chloroperoxybenzoic acid in water (0.92 mmol of mCPBA) was added. After stirring for 16 hrs at room 186 temperature, the reaction mixtures were added to a separatory funnel, the organic layers were washed 187 with a 0.5 N aqueous NaOH solution (5 x 4 mL) and brine (2 x 3 mL). Finally, the organic layers were 188 dried over anhydrous Na<sub>2</sub>SO<sub>4</sub>, filtered, and concentrated under reduced pressure to afford the 189 electrophilic methyl sulfones in 93–95% yield (see also Scheme 1). The activated sulfones were carried 190 forward for the IEG coupling steps without further purification.

Coupling of Active IEG Units: The methyl sulfone oligomers (0.26 mmol) and K<sub>2</sub>CO<sub>3</sub> (0.55 mmol) were added to a flame-dried, 5 ml round-bottomed flask under a nitrogen atmosphere, and anhydrous DMF (4 mL) was added. Next, the oligomers with the free phenolic ends (0.18 mmol) were added to the reaction mixtures at room temperature. Afterwards, the reaction mixtures were warmed to 40 °C and stirred at 40 °C for 12 hrs. Finally, the reaction mixtures were diluted with a 0.5 N aqueous HCl solution (5 mL), transferred to a separatory funnel, and extracted with EtOAc (3 x 5 mL). The combined organic phases were washed with brine (3 x 3 mL) as well as with a 0.5 N aqueous NaOH solution (2 x 3 mL) to ensure that any potentially remaining phenol was removed. Finally, the combined organic layers were dried over anhydrous Na<sub>2</sub>SO<sub>4</sub>, filtered, and concentrated under reduced pressure. The crude products were purified via flash-column chromatography over silica gel (eluent: 0–15% ethyl acetate in hexanes) to afford the coupled IEG products 4, 5, and 6 in a 48–98% yield (see also Scheme 1). For the hexadecameric product 6, the yield was determined from a quantitative <sup>1</sup>H NMR spectrum obtained from the crude reaction mixture (in the presence of dimethyl sulfone as the internal standard for <sup>1</sup>H NMR integration) since a significant amount of material was lost during silica-column chromatography purification as a result of the reduced solubility of this relatively large oligomer in the purification solvent. In general, we found that reduced solubility in hexanes of the IEG polymers with increasing lengths presented a challenge for purification of the compounds via chromatographic methods, which resulted in variable yields for the purified products.

#### 3.3 Single Crystal X-Ray Crystallography

191

192

193

194

195

196

197

198

199

200

201

202

203

204

205

206

207

208

209

211

210 Single crystals of 3 were grown by slow vapor diffusion of hexanes into ethyl acetate solutions of 3. Intensity data were collected on a Bruker D8 Venture kappa diffractometer equipped with a Photon II 212 detector. An Iµs microfocus source provided the Mo K $\alpha$  radiation ( $\lambda = 0.71073$  A) that was 213 monochromated with multilayer mirrors. The collection, cell refinement and integration of intensity

- data were carried out with the APEX3 software (Bruker, 2018). Face-indexed absorption corrections
- were performed using multi-scan methods using SADABS (Krause et al., 2015). The initial structure
- solution was solved with the intrinsic phasing methods SHELXT (Sheldrick, 2015b) and refined with
- 217 the full-matrix least-squares SHELXL(Sheldrick, 2015a) program. The 1 3 5 and -2 5 4 reflections
- were omitted from the final refinement due to being partially obscured by the beam stop in some
- 219 orientations.

224

239

- 220 Crystal data for 3:  $C_{12}H_{12}N_2O_2S$ ,  $M_r = 248.30$ , crystal size 0.374 x 0.363 x 0.254 mm<sup>3</sup>, monoclinic,
- 221 space group  $P2_1/n$ , a = 7.9829(5), b = 14.2529(8), c = 20.6830(11) Å,  $\alpha = 90^\circ$ ,
- 222  $\beta = 91.442(2)^{\circ}, \gamma = 90^{\circ}, V = 2352.6(2)$  Å<sup>3</sup>, Z = 8,  $\rho_{calcd} = 1.402$  mg m<sup>-3</sup>, T = 100 (2) K,
- 223  $R_1[F^2 > 2\sigma(F^2)] = 0.0288, wR_2 = 0.0790.$

# 3.4 Density Functional Theory

- All structures were optimized with the Jaguar software package at the B3LYP-D3/6-31G\*\* and
- B3LYP-D3/6-31G\*\* levels (for the NCI critical point calculations) of theory. NCI critical points of
- 227 the electron density were calculated with the Jaguar software package at the B3LYP-D3/6-31G\*\* level.

# 228 4 Conclusions

- 229 This work demonstrates a unique iterative exponential growth (IEG) technique, which employs
- 230 nucleophilic aromatic substitution (S<sub>N</sub>Ar) reactions as a tool to fabricate architecturally defined
- conjugated ABAB polymers with a metal-free coupling strategy. The monomers are designed to exhibit
- both nucleophilic and electrophilic character, either of which can be accessed selectively via
- 233 deprotection of methoxyl groups and via oxidation of aromatic sulfides. Integrating S<sub>N</sub>Ar reactions
- with iterative exponential growth eliminates the need for expensive transition metal catalysts, which
- have been required so far in order to carry out iterative exponential growth of conjugated and/or
- 236 unimolecular, heteroatom-linked aromatic polymers. Our transition metal free IEG methodology
- 237 allowed us to access heteroatom-linked, unimolecular aromatic polymers with up to 16 alternating
- 238 resorcinol and pyrimidine units, enabling us to investigate, for the first time, the [CH···O] hydrogen-

bond driven folding of such polymers with single crystal X-ray crystallography, <sup>1</sup>H-<sup>1</sup>H NOESY NMR

- spectroscopy, and density functional theory (DFT). Overall, our new IEG methodology advances
- fundamental capacity to access new unimolecular polymers needed to investigate the diverse physical
- and electronic properties of heteroatom-linked polyaromatic systems. We are currently applying our

- 243 new transition metal-free IEG methodology to longer precision polymers with extended solubilizing
- 244 chains.

### 245 5 Data Availability Statement

- 246 The crystal data for the single crystal X-ray structure reported in this paper have been deposited in the
- 247 Cambridge Crystallographic Data Centre (CCDC: 2036161). The raw NMR and mass spectral datasets
- 248 generated for this study are available from the corresponding author on request.

#### 249 **6** Author Contributions

- TJJ, MS, JPC, and STS wrote the paper. STS obtained funding for the project. TJJ, MS, JPC, JB, KTM;
- 251 KL, and ROB conducted the experiments. DLG and TJW solved the crystal structure reported in the
- paper. All authors helped analyse the data and revise the paper.

# **253 7 Funding**

- 254 The synthesis of the IEG synthesis of the polymers was supported by the National Science Foundation
- 255 (Grant CHE-1609137 awarded to STS) as well as by UVM Chemistry, SURF, and Biochemistry
- 256 undergraduate research fellowship grants awarded to TJJ, KL, and ROB. JL was partially supported
- by the ACS Petroleum Research Fund (58219-DNI). The folding studies of the sequence-defined IEG
- 258 polymers were supported by the Army Research Office (Grant 71015-CH-YIP awarded to STS). The
- 259 UVM Mass Spectrometry facilities were supported by National Institutes of Health (Grants S10-
- 260 OD018126 and P30-GM118228).

#### 261 8 Acknowledgments

263

264

269

We thank B. O Rourke for high-resolution mass spectrometry.

#### 9 Supplementary Material

#### 266 **10** Conflict of Interest

- The authors declare that the research was conducted in the absence of any commercial or financial
- relationships that could be construed as a potential conflict of interest.

#### 11 References

Adhikari, B., Yamada, Y., Yamauchi, M., Wakita, K., Lin, X., Aratsu, K., Ohba, T., Karatsu, T., Hollamby, M.J., Shimizu, N., Takagi, H., Haruki, R., Adachi, S.I., and Yagai, S. (2017). Light-induced unfolding and refolding of supramolecular polymer nanofibres. *Nat. Commun* 8, 15254.

Barnes, J.C., Ehrlich, D.J., Gao, A.X., Leibfarth, F.A., Jiang, Y., Zhou, E., Jamison, T.F., and Johnson, J.A. (2015). Iterative exponential growth of stereo- and sequence-controlled polymers. *Nat. Chem.* 7, 810-815.

Becke, A.D. (1993). Density-functional thermochemistry. III. The role of exact exchange. *J. Chem. Phys.* 98, 5648-5652.

Beugelmans, R., Singh, G.P., Bois-Choussy, M., Chastanet, J., and Zhu, J. (1994). SNAr-based macrocyclization: an application to the synthesis of vancomycin family models. *J. Org. Chem.* 59, 5535-5542.

Binauld, S., Damiron, D., Connal, L.A., Hawker, C.J., and Drockenmuller, E. (2011). Precise synthesis of molecularly defined oligomers and polymers by orthogonal iterative divergent/convergent approaches. *Macromol. Rapid. Commun.* 32, 147-168.

Blaziak, K., Danikiewicz, W., and Makosza, M. (2016). How does nucleophilic aromatic substitution really proceed in nitroarenes? computational prediction and experimental verification. *J. Am. Chem. Soc.* 138, 7276-7281.

Bochevarov, A.D., Harder, E., Hughes, T.F., Greenwood, J.R., Braden, D.A., Philipp, D.M., Rinaldo, D., Halls, M.D., Zhang, J., and Friesner, R.A. (2013). Jaguar: A high-performance quantum chemistry software program with strengths in life and materials sciences. Int. *J. Quantum Chem.* 113, 2110-2142.

Bonduelle, C. (2018). Secondary structures of synthetic polypeptide polymers. *Polym. Chem* 9, 1517-1529.

Bruker (2018). APEX3. Bruker AXS, Inc., Madison, Wisconsin, USA.

Chen, L., Wang, H., Zhang, D.W., Zhou, Y., and Li, Z.T. (2015). Quadruple switching of pleated foldamers of tetrathiafulvalene-bipyridinium alternating dynamic covalent polymers. *Angew. Chem. Int. Ed.* 54, 4028-4031.

Cole, J.P., Hanlon, A.M., Rodriguez, K.J., and Berda, E.B. (2017). Protein-like structure and activity in synthetic polymers. *J. Polym. Sci., Part A: Polym. Chem* 55, 191-206.

Delawder, A.O., Natraj, A., Colley, N.D., Saak, T., Greene, A.F., and Barnes, J.C. (2019). Synthesis, self-assembly, and photomechanical actuator performance of a sequence-defined polyviologen crosslinker. *Supramol Chem* 31, 523-531.

Dobscha, J.R., Castillo, H.D., Li, Y., Fadler, R.E., Taylor, R.D., Brown, A.A., Trainor, C.Q., Tait, S.L., and Flood, A.H. (2019). Sequence-defined macrocycles for understanding and controlling the build-up of hierarchical order in self-assembled 2D arrays. *J. Am. Chem. Soc.* 141, 17588-17600.

Gerthoffer, M.C., Wu, S., Chen, B., Wang, T., Huss, S., Oburn, S.M., Crespi, V.H., Badding, J.V., and Elacqua, E. (2020). 'Sacrificial' supramolecular assembly and pressure-induced polymerization: toward sequence-defined functionalized nanothreads. *Chem. Sci.* 

Goodman, C.M., Choi, S., Shandler, S., and Degrado, W.F. (2007). Foldamers as versatile frameworks for the design and evolution of function. *Nat. Chem. Biol.* 3, 252-262.

Grayson, S.M., and Frechet, J.M. (2001). Convergent dendrons and dendrimers: from synthesis to applications. *Chem. Rev.* 101, 3819-3868.

Greene, A.F., Danielson, M.K., Delawder, A.O., Liles, K.P., Li, X., Natraj, A., Wellen, A., and Barnes, J.C. (2017). Redox-responsive artificial molecular muscles: reversible radical-based self-assembly for actuating hydrogels. *Chem. Mater.* 29, 9498-9508.

Guan, Y., Wang, C., Wang, D., Dang, G., Chen, C., Zhou, H., and Zhao, X. (2015). Methylsulfone as a leaving group for synthesis of hyperbranched poly(arylene pyrimidine ether)s by nucleophilic aromatic substitution. *RSC Adv.* 5, 12821-12823.

Hanlon, A.M., Martin, I., Bright, E.R., Chouinard, J., Rodriguez, K.J., Patenotte, G.E., and Berda, E.B. (2017). Exploring structural effects in single-chain "folding" mediated by intramolecular thermal Diels–Alder chemistry. *Polym. Chem* 8, 5120-5128.

Harder, E., Damm, W., Maple, J., Wu, C., Reboul, M., Xiang, J.Y., Wang, L., Lupyan, D., Dahlgren, M.K., Knight, J.L., Kaus, J.W., Cerutti, D.S., Krilov, G., Jorgensen, W.L., Abel, R., and Friesner, R.A. (2016). OPLS3: A force field providing broad coverage of drug-like small molecules and proteins. *J. Chem. Theory. Comput.* 12, 281–296.

Hawker, C.J., Malmström, E.E., Frank, C.W., and Kampf, J.P. (1997). Exact linear analogs of dendritic polyether macromolecules: design, synthesis, and unique properties. *J. Ame. Chem. Soc* 119, 9903-9904.

Huang, Z., Zhao, J., Wang, Z., Meng, F., Ding, K., Pan, X., Zhou, N., Li, X., Zhang, Z., and Zhu, X. (2017). Combining orthogonal chain-end deprotections and thiol-maleimide Michael coupling: engineering discrete oligomers by an iterative growth strategy. *Angew. Chem. Int. Ed.* 56, 13612-13617.

Johnson, E.R., Keinan, S., Mori-Sanchez, P., Contreras-Garcia, J., Cohen, A.J., and Yang, W. (2010). Revealing noncovalent interactions. *J. Am. Chem. Soc.* 132, 6498-6506.

Jones, L., Schumm, J.S., and Tour, J.M. (1997). Rapid solution and solid phase syntheses of oligo(1,4-phenylene)s with thioester termini: molecular scale wires with alligator clips. derivation of iterative reaction efficiencies on a polymer support. *J. Org. Chem* 62, 1388-1410.

Krause, L., Herbst-Irmer, R., Sheldrick, G.M., and Stalke, D. (2015). Comparison of silver and molybdenum microfocus X-ray sources for single-crystal structure determination. *J. Appl. Crystallogr* 48, 3-10.

Landovsky, T., Eigner, V., Babor, M., Tichotova, M., Dvorakova, H., and Lhotak, P. (2019). Regioselective SNAr reaction of the phenoxathiin-based thiacalixarene as a route to a novel macrocyclic skeleton. *Chem Commun* 56, 78-81.

Lee, C., Yang, W., and Parr, R.G. (1988). Development of the Colle-Salvetti correlation-energy formula into a functional of the electron density. *Phys. Rev. B.* 37, 785-789.

- Leibfarth, F.A., Johnson, J.A., and Jamison, T.F. (2015). Scalable synthesis of sequence-defined, unimolecular macromolecules by Flow-IEG. *Proc. Natl. Acad. Sci. U.S.A.* 112, 10617-10622.
- Li, G., Wang, X., and Wang, F. (2005). A novel in situ deprotection/coupling and iterative divergent/convergent strategy for the synthesis of oligo(1,4-phenyleneethynylene)s. *Tetrahedron. Lett.* 46, 8971-8973.
- Li, G., Nieves-Quinones, Y., Zhang, H., Liang, Q., Su, S., Liu, Q., Kozlowski, M. C., and Jia, T. (2020). Transition-metal-free formal cross-coupling of aryl methyl sulfoxides and alcohols via nucleophilic activation of C-S bond. *Nature Commun.* 11, 2890.
- Liess, P., Hensel, V., and Schlüter, A.D. (2006). Oligophenylene Rods: A Repetitive Approach. *Liebigs. Annalen.* 1996, 1037-1040.
- Liu, X., Weinert, Z.J., Sharafi, M., Liao, C., Li, J., and Schneebeli, S.T. (2015). Regulating molecular recognition with c-shaped strips attained by chirality-assisted synthesis. *Angew. Chem. Int. Ed.* 54, 12772-12776.
- Louie, J., and Hartwig, J.F. (1998). The Largest Discrete Oligo(m-aniline). An Exponential growth strategy using palladium-catalyzed amination of aryl sulfonates. Macromolecules 31, 6737-6739.
- Ong, W.J., and Swager, T.M. (2018). Dynamic self-correcting nucleophilic aromatic substitution. *Nat Chem* 10, 1023-1030.
- Otte, M. (2016). Size-selective molecular flasks. ACS. Catal. 6, 6491-6510.
- Rajappan, S.C., Mccarthy, D.R., Campbell, J.P., Ferrell, J.B., Sharafi, M., Ambrozaite, O., Li, J., and Schneebeli, S.T. (2020). Selective monofunctionalization enabled by reaction history-dependent communication in catalytic rotaxanes. *Angew. Chem. Int. Ed.* 10.1002/anie.202006305.
- Read, M.W., Escobedo, J.O., Willis, D.M., Beck, P.A., and Strongin, R.M. (2000). Convenient iterative synthesis of an octameric tetracarboxylate-functionalized oligophenylene rod with divergent end groups. *Org. Lett.* 2, 3201-3204.
- Sadighi, J.P., Singer, R.A., and Buchwald, S.L. (1998). Palladium-catalyzed synthesis of monodisperse, controlled-length, and functionalized oligoanilines. *J. Am. Chem. Soc.* 120, 4960-4976.
- Schneebeli, S., Li, J., Sharafi, M., Weinert, Z., Cohen, I., Liao, C., and Ivancic, M. (2016). Controlled self-assembly inside c-shaped polyaromatic strips. *Synlett* 27, 2145-2149.
- Sharafi, M., Mckay, K.T., Ivancic, M., Mccarthy, D.R., Dudkina, N., Murphy, K.E., Rajappan, S.C., Campbell, J.P., Shen, Y., Badireddy, A.R., Li, J., and Schneebeli, S.T. (2020). Size-selective catalytic polymer acylation with a molecular tetrahedron. *Chem* 6, 1469-1494.
- Sheldrick, G.M. (2015a). Crystal structure refinement with SHELXL. Acta. Cryst. C 71, 3-8.
- Sheldrick, G.M. (2015b). SHELXT integrated space-group and crystal-structure determination. *Acta Cryst. A* 71, 3-8.
- Sun, C.-L., and Shi, Z.-J. (2014). Transition-metal-free coupling reactions. *Chem. Rev.* 114, 9219-9280.

Van Rossom, W., Caers, J., Robeyns, K., Van Meervelt, L., Maes, W., and Dehaen, W. (2012). (Thio)ureido anion receptors based on a 1,3-alternate oxacalix[2]arene[2]pyrimidine scaffold. *J. Org. Chem* 77, 2791-2797.

Xie, J., Li, X., Wang, S., Li, A., Jiang, L., and Zhu, K. (2020). Heteroatom-bridged molecular belts as containers. *Nat. Commun* 11, 3348.

Zhang, J., Moore, J.S., Xu, Z., and Aguirre, R.A. (1992). Nanoarchitectures. 1. Controlled synthesis of phenylacetylene sequences. *J. Am. Chem. Soc.* 114, 2273-2274.

Zhao, W., Qiao, B., Tropp, J., Pink, M., Azoulay, J.D., and Flood, A.H. (2019). Linear supramolecular polymers driven by anion-anion dimerization of difunctional phosphonate monomers inside cyanostar macrocycles. *J. Am. Chem. Soc.* 141, 4980-4989.

Zhao, W., Tropp, J., Qiao, B., Pink, M., Azoulay, J.D., and Flood, A.H. (2020). Tunable adhesion from stoichiometry-controlled and sequence-defined supramolecular polymers emerges hierarchically from cyanostar-stabilized anion-anion linkages. *J. Am. Chem. Soc.* 142, 2579-2591.

#### 12 Scheme and Figure Captions

Figure 1. Comparison of previously reported transition metal (TM) catalyzed IEG methods to our TM-free strategy for the construction of well-defined polyaromatic precision macromolecules. Our approach eliminates the need for transition metal catalysts by introducing methyl sulfones as efficient leaving groups for  $S_N$ Ar-based IEG processes.

**Scheme 1.** Synthesis of unimolecular polymers with alternating resorcinol and pyrimidine units with S<sub>N</sub>Ar-baseed IEG couplings, based on masking/unmasking via methyl sulfide to methyl sulfone oxidation. The general reaction conditions for deprotection/activation, and IEG coupling are the following: (a) Coupling: K<sub>2</sub>CO<sub>3</sub>, DMF, 60 °C, 12 hrs, room temperature. (b) Deprotection of terminal methoxyl groups to generate nucleophilic phenols: BBr<sub>3</sub>, CH<sub>2</sub>Cl<sub>2</sub>, –78 °C to room temperature, 12 hrs. (c) Activation of methyl sulfides to generate electrophilic methyl sulfones: *m*CPBA, EtOAc, room temperature, 24 hrs.

**Figure 2.** (**A and B**) Single crystal X-ray structure of 4-(3-methoxyphenoxy)-6-(methylthio)pyrimidine (**3**). (C) DFT-optimized structure (B3LYP/6-31G\*\* level) of a model hydrogen-bonded dimer, 1,3-dimethoxyphenol in complex with 4-methoxy-6-(methylthio)pyrimidine. NCI critical points of the electron density (calculated at the B3LYP/6-31G\*\* level of theory) are illustrated with blue spheres. Color code: C: gray; H: white; N: blue; O: red; S; yellow.

**Figure 3. (A)** Partial <sup>1</sup>H-<sup>1</sup>H NOESY NMR (500 MHz, CDCl<sub>3</sub>, 298 K) of the hexadecamer **6**. The key NOE cross peak, which is consistent with polymer folding, is highlighted with an arrow. **(B)** Corresponding model of a potential folded structure of compound **6**. The structure shown represents the lowest energy conformation found with a MacroModel conformational search (OPLS3e force field), which was then refined with a DFT optimization at the B3LYP-D3/6-31G\*\* level of theory.

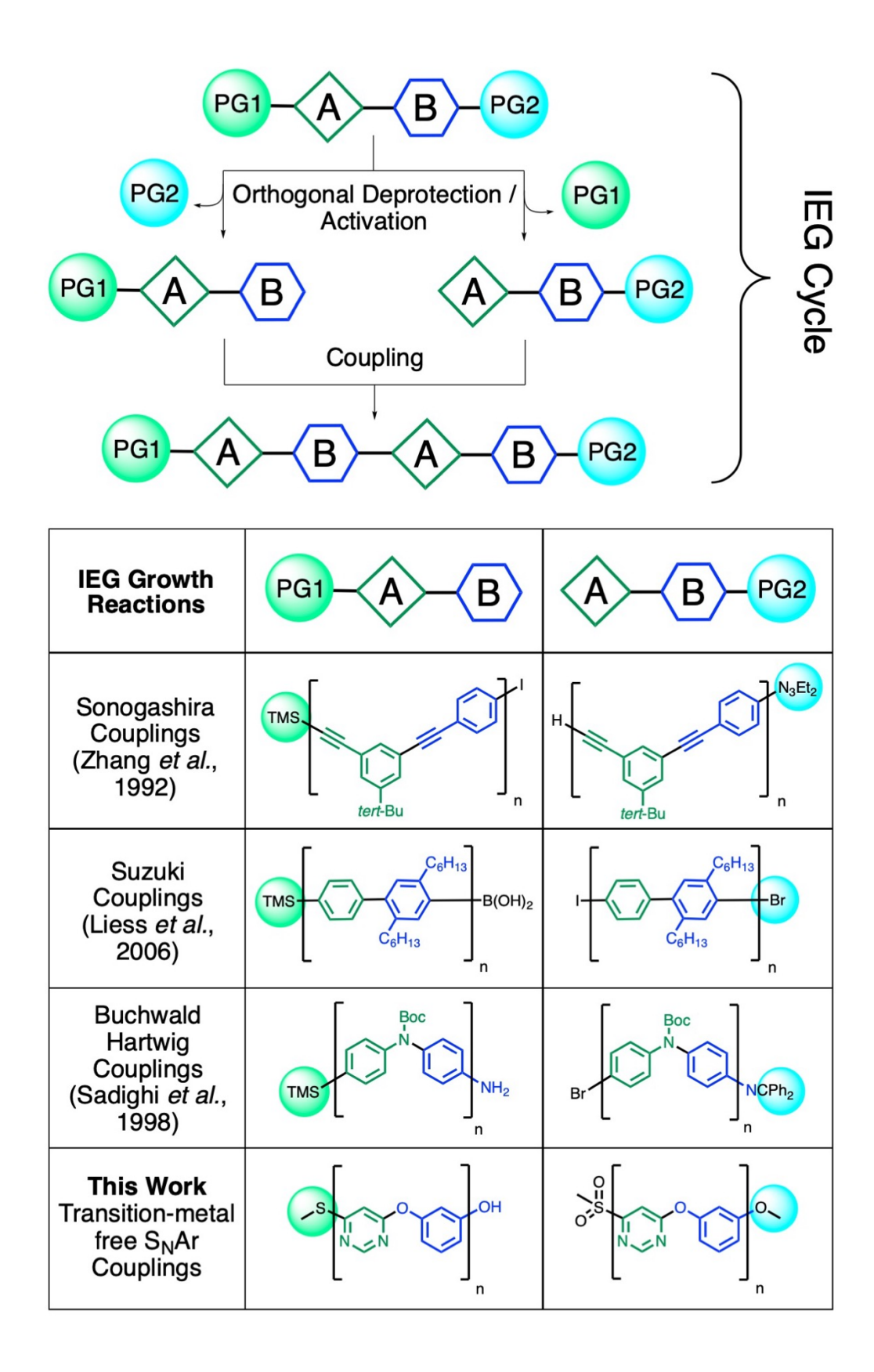
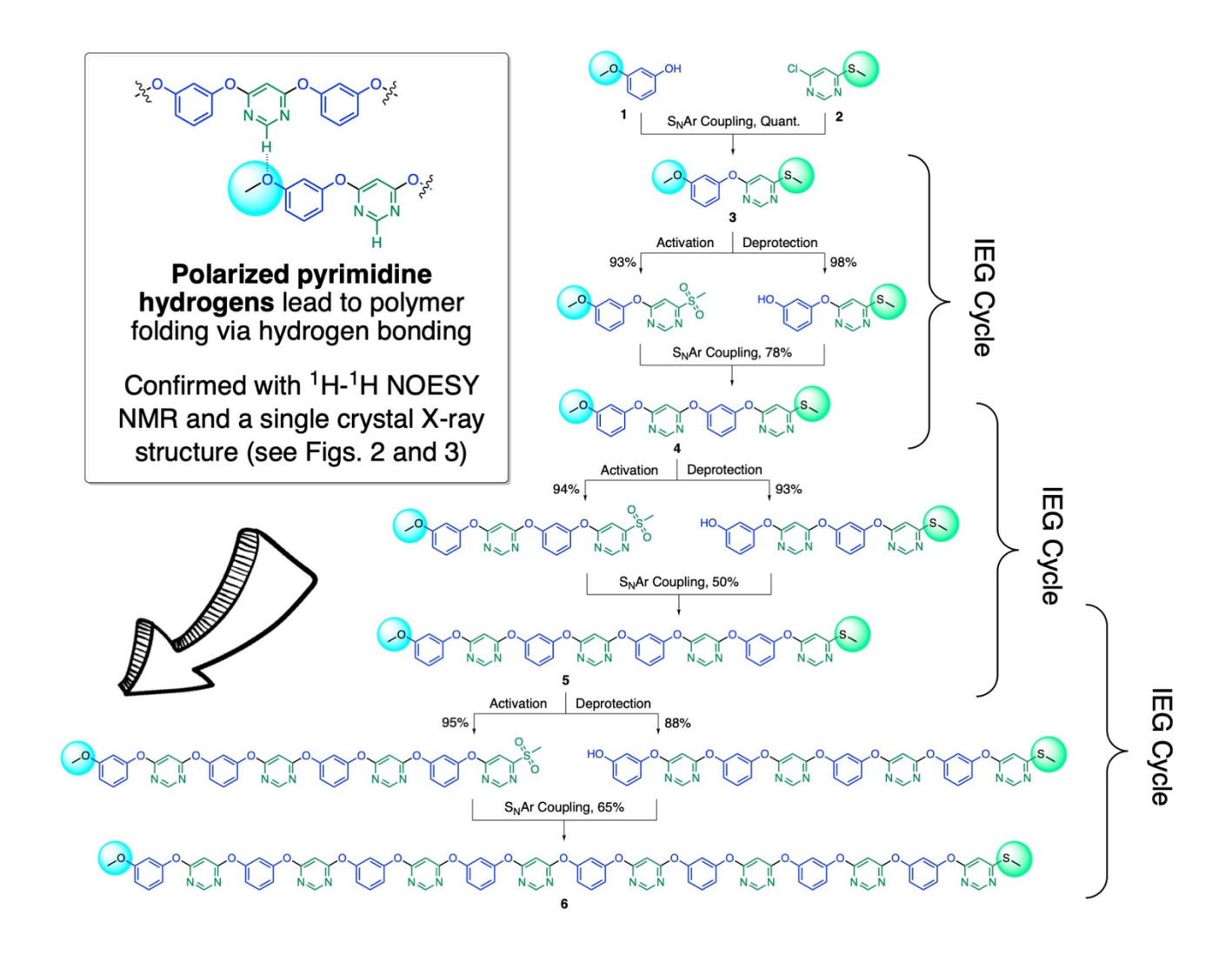


Figure 1



Scheme 1

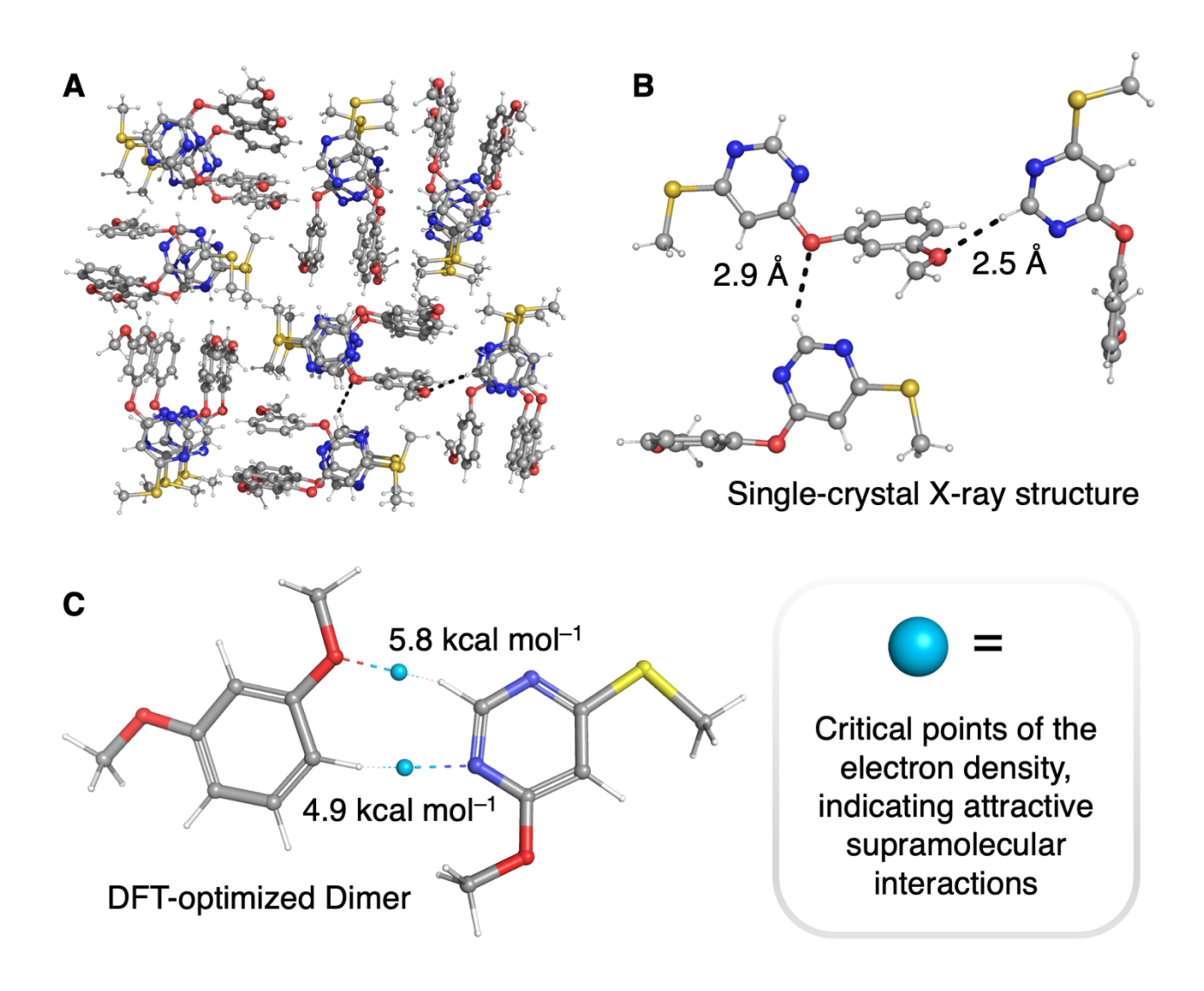


Figure 2

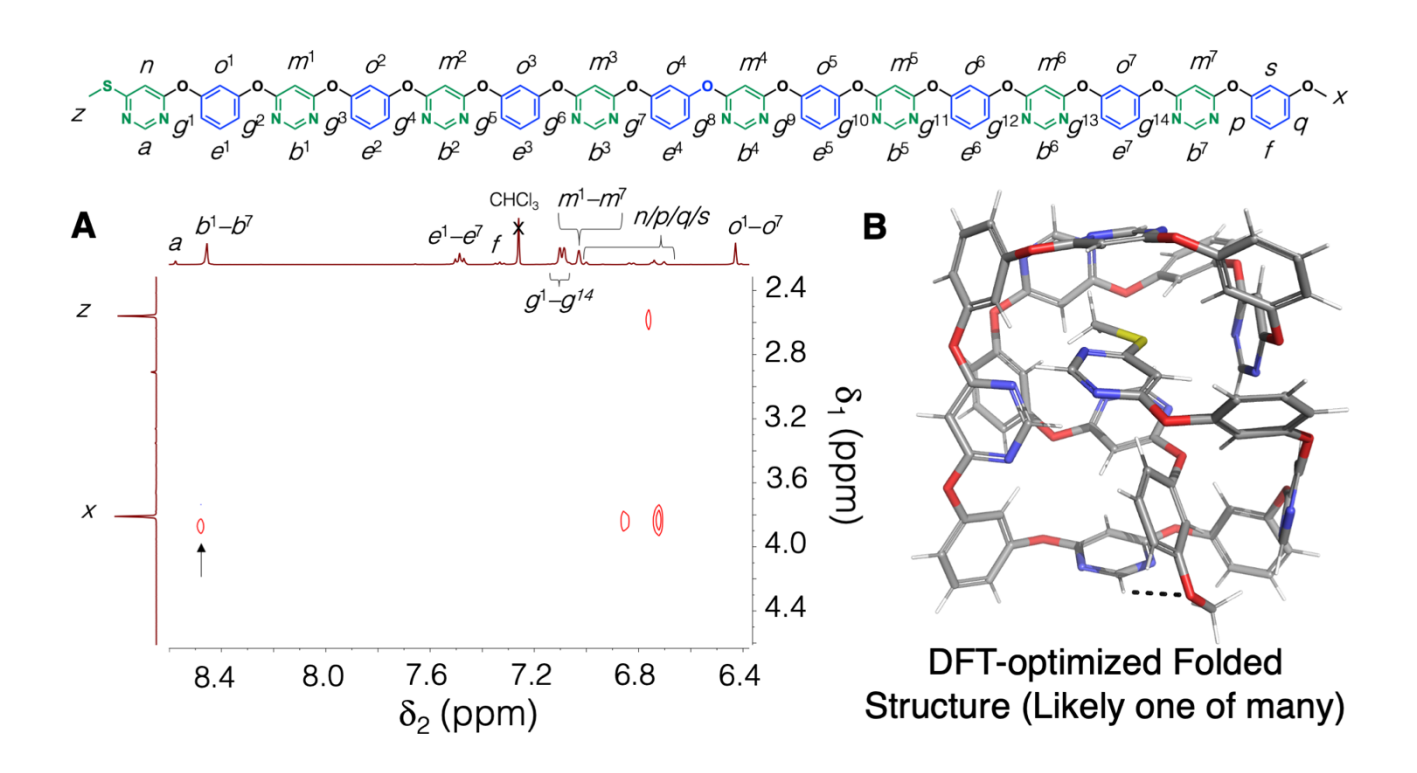


Figure 3